Photodissociation dynamics of HCl in solid Ar: Cage exit, nonadiabatic transitions, and recombination

Anna I. Krylov[a] and R. Benny Gerber
Department of Physical Chemistry and The Fritz Haber Research Center, The Hebrew University, Jerusalem 91904, Israel and Department of Chemistry, University of California, Irvine, California 92697

(Received 4 November 1996; accepted 22 January 1997)

The photodissociation of HCl in solid Ar is studied by non-adiabatic Molecular Dynamics simulations, based on a surface-hopping treatment of transitions between different electronic states. The relevant 12 potential energy surfaces and the non-adiabatic interactions between them were generated by a Diatomics-in-Molecules (DIM) approach, which incorporated also spin-orbit coupling. The focus of the study is on the non-adiabatic transitions, and on their role both in the cage-exit of the H atom, and in the recombination process. It is found that non-adiabatic transitions occur very frequently. In some of the trajectories, all the 12 electronic states are visited during the timescale studied. At least one non-adiabatic transition was found to occur even in the fastest cage-exit events. The other main results are: (1) The total yields for photofragment separation (by cage exit of the H atom) and for H+Cl recombination onto the ground state are roughly equal in the conditions used. (2) The cage exit events take place in the time-window between ~70 fs and ~550 fs after the excitation pulse, and are thus all at least somewhat delayed. The recombination events span a much broader time-window, from almost immediately after excitation, and up to ~1100 fs and beyond. (3) The electronic energy relaxation events during the process depend significantly on symmetry and interactions of the states involved, and not only on the energy gaps between them. (4) Different electronic states reached in the course of the process exhibit different propensities with regard to the recombination versus cage exit outcome. (5) Spin-orbit interactions, and spin-forbidden transitions play an important role in the process, especially for recombination events. © *1997 American Institute of Physics.* [S0021-9606(97)01916-8]

I. INTRODUCTION

Cage effects and geminate recombination are amongst the most important concepts in condensed-phase chemical dynamics, and had been the topics of extensive experimental and theoretical studies throughout the years. In the past two decades, there has been growing interest in exploring these phenomena in the context of photochemical processes for small guest molecules in a solid rare-gas environment.[1–23] Experimentally, these systems have the advantage of several convenient optical properties, especially the spectroscopic transparency of the host rare gas solid in the relevant regions. Among the important experimental developments of recent years, there was the application of synchrotron excitation techniques by Schwentner and coworkers[8–14] which made it possible to access the dissociation bands of an increased number of small molecules of interest. Another important new direction was pioneered by Apkarian and coworkers[20–22] who applied time-domain femtosecond pulse spectroscopy to study the cage effect for molecules in rare-gas solids. Theoretically, these systems are attractive because the interaction potentials between the reactive molecular species and the solid host atoms are relatively simple and often available. Another advantage of these systems is that at least the initial structure around the reagent, prior to photoexcitation, is typically well defined and can simplify the task of interpretation. Classical Molecular Dynamics simulations were first applied to microscopic modeling of molecular photodissociation in solids, and to the corresponding reactions in large rare-gas clusters, almost ten years ago,[24,25] and have since emerged as an extremely useful tool for gaining detailed insight into the dynamics of these processes.[24–36] Such simulations were able, for instance, to provide interpretation for experiments on cage exit following photodissociation of F_2 (Ref. 30) and of Cl_2 (Ref. 31) in rare gas solids. Indeed, Molecular Dynamics simulations were able to reproduce many of the quantitative experimental features associated with the coherent cage vibrations of I_2 in rare-gas solids measured by ultrafast spectroscopy techniques.[20–22] While theoretical modeling of cage processes confined to a single potential energy surface has been extensively pursued, this is not the case for non-adiabatic processes taking place for a molecule in a matrix. Realistically, however, most if not all of the systems studied in the context of molecular photochemistry in rare-gas solids involve some non-adiabatic processes, and these processes may play an important role on the timescale of the experiment of interest. A molecule excited to a dissociative state in a medium, beginning to separate into fragments, can with some probability undergo electronic relaxation, possibly reaching its ground state and recombining on it. Only very few quantitative theoretical studied were hitherto made of these extremely important processes. Semiclassical methods, rather than classical dynamics, must obviously be used in describing such non-adiabatic

[a]Present address: Department of Chemistry, University of California, Berkeley, California 94720.

processes. Most related to the present work are the non-adiabatic simulations of Gersonde and Gabriel[37] of photolysis and recombination of diatomic molecules in rare-gas solids, and the study of Batista and Coker[38] on non-adiabatic processes in the caging of I_2 in liquid Xe.

The purpose of the present article is to explore the non-adiabatic dynamics following excitation of HCl to a dissociative state in solid Ar. We shall study the competition between H-atom cage exit, leading to ''permanent'' separation of the photofragments and the process of recombination, resulting in electronic ground state HCl. Of central interest will be the pathways of cascading through the large manifold of electronic states involved, until the ground state is reached. We shall study by non-adiabatic simulations the physical mechanisms whereby such processes occur, and the nature of the interactions that govern the transitions between different electronic states. Important differences will be recognized between the present system as simulated here, and the processes studied in Refs. 37 and 38. We chose HCl partly because of the interesting properties of hydrogen as a (small) photofragment, and partly because photolysis of HCl, and other hydrogen halides in solids has already received considerable experimental attention.[13,14,19,34]

The structure of the paper is as follows: Sec. II describes the system, the interaction potentials, and the non-adiabatic simulation method. Sec. III outlines the main findings and provides analysis. Concluding remarks are presented in Sec. IV.

II. SYSTEM AND METHODS

The simulations described in this study were carried out for systems consisting of 255 Ar atoms and a HCl molecule, initially placed at a substitutional site of the argon lattice. Periodic boundary conditions were imposed at the ends of the system. On the basis of previous simulations of photophysical and photochemical processes in solids, it is expected to be sufficient in size to describe the processes of interest without giving rise to noticeable unphysical ''finite size'' effects.

A. Potential surfaces

The potential surfaces for the system were constructed by a variant of the DIM (Diatomics in Molecules)[39] method. The DIM approach was used by the present authors and coworkers for the related topic of open shell, P-state atoms such as $F(^2P)$,[40,41] $Cl(^2P)$,[42] and $Ba(P)$ (Ref. 43) in a rare-gas environment. The DIM method was used by Batista and Coker, in their study of I_2 in liquid Xe,[38] by Buchachenko and Stepanov, in their study of I_2Ar,[44] and previously by Gersonde and Gabriel[37] in simulations of photolysis of several diatomics in rare gas solids, but the latter authors did not include spin-orbit interactions in their version of the method.

Consider first the HCl part of the system. There are 12 states, including degeneracies and the ground state, that dissociate asymptotically to $H(^1S)+Cl(^2P)$. Using an effective one-electron model for the $Cl(^2P)$ atom, and a Valence-Bond approach, the 12 states can be written explicitly as a combination of the s-orbital of the H, and p-orbitals of the Cl atom. The ground state $^1\Sigma_0$ is:

$$^1\Sigma_0=\frac{1}{2}[s(1)p_0(2)+p_0(1)s(2)][\alpha(1)\beta(2) - \beta(1)\alpha(2)], \tag{1}$$

where p_0 is the p-orbital corresponding to the angular momentum projection $m_L=0$. The $^3\Sigma_1$ states are:

$$\begin{aligned} ^3\Sigma_1&=\frac{1}{\sqrt{2}}[s(1)p_0(2)-p_0(1)s(2)]\alpha(1)\alpha(2),\\ ^3\Sigma_1&=\frac{1}{\sqrt{2}}[s(1)p_0(2)-p_0(1)s(2)]\beta(1)\beta(2),\\ ^3\Sigma_0&=\frac{1}{\sqrt{2}}[s(1)p_0(2)-p_0(1)s(2)] \times\left[\frac{1}{\sqrt{2}}(\alpha(1)\beta(2)+\beta(1)\alpha(2))\right]. \end{aligned} \tag{2}$$

For the Π states, we write for convenience the spatial part only:

$$\begin{aligned} ^1\Pi(m_L=-1)&=\frac{1}{\sqrt{2}}[sp_{-1}+p_{-1}s],\\ ^3\Pi(m_L=-1)&=\frac{1}{\sqrt{2}}[sp_{-1}-p_{-1}s],\\ ^1\Pi(m_L=1)&=\frac{1}{\sqrt{2}}[sp_1+p_1s],\\ ^3\Pi(m_L=1)&=\frac{1}{\sqrt{2}}[sp_1-p_1s]. \end{aligned} \tag{3}$$

For nomenclature purposes it will be useful to order the VB basis functions. We will use the order: $^1\Pi_{-1}$, $^1\Sigma_0$, $^1\Pi_{+1}$, $^3\Pi_0$, $^3\Sigma_{+1}$, $^3\Pi_{+2}$, $^3\Pi_{-1}$, $^3\Sigma_0$, $^3\Pi_{+1}$, $^3\Pi_{-2}$, $^3\Sigma_{-1}$, $^3\Pi_0$. The first three states in this sequence are the singlets, the following three states are triplet states of spin functions $\alpha(1)\alpha(2)$, the next three states correspond to spin functions $(1/\sqrt{2})(\alpha\beta+\beta\alpha)$, and the last three states have $\beta\beta$ spin functions. The above order is not necessarily that of increasing energy. The potential energy curves of HCl corresponding to some of these states are shown in Fig. 1. These curves, taken from the ab initio calculations of Bettendorff *et al.*,[45] were used in obtaining the DIM potential surfaces, as discussed below. The DIM electronic Hamiltonian of the system can be written in the form:

$$\begin{aligned} H_{\rm el}(\gamma,\mathbf{R})&=H^{\rm el}_{\rm HCl}(\gamma,R_{HCl})+V_{\rm HAr}(\mathbf{R}_{\rm H},\mathbf{R}_1,\ldots,\mathbf{R}_N)\\ &\quad+V_{ClAr}(\gamma,\mathbf{R}_{\rm Cl},\mathbf{R}_1,\ldots,\mathbf{R}_N)\\ &\quad+V_{\rm ArAr}(\mathbf{R}_1,\ldots,\mathbf{R}_N)+\hat{V}_{\rm SO}, \end{aligned} \tag{4}$$

where γ denotes collectively the electronic degrees of freedom; $\mathbf{R}$—the nuclear coordinates, $\mathbf{R}_1,\ldots,\mathbf{R}_N$ are the position vectors of the Ar atoms, $\mathbf{R}_{\rm H},\mathbf{R}_{\rm Cl}$ are the positions of the H and the Cl atoms, respectively, and $R_{\rm HCl}=|\mathbf{R}_{\rm H}-\mathbf{R}_{\rm Cl}|$. $H^{\rm el}_{\rm HCl}(\gamma,R_{\rm HCl})$ is the electronic Hamiltonian of the isolated

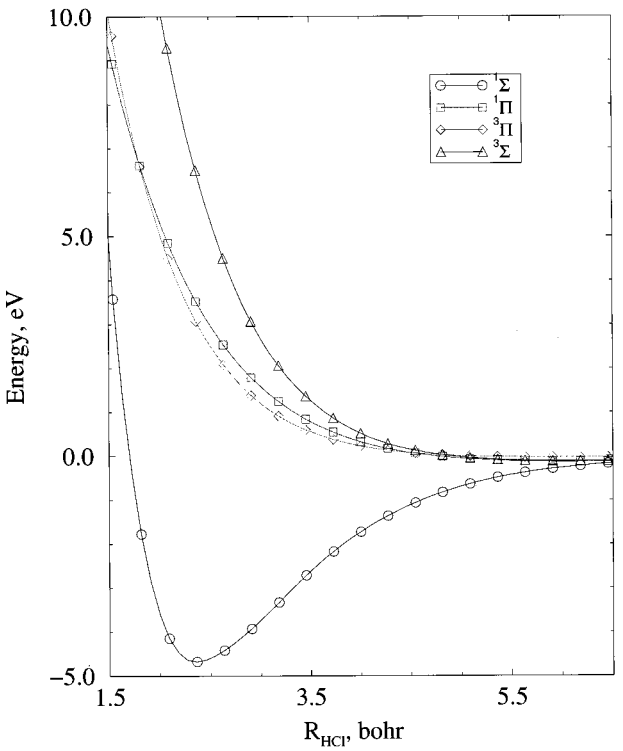

FIG. 1. Potential energy curves of HCl (see text).

HCl molecule. We assume that its eigenfunctions are given to good approximation by the Valence Bond model of Eqs. (1)–(3). For the eigenvalues of $H^{\mathrm{el}}_{\mathrm{HCl}}$, $W^{\mathrm{HCl}}_n(R_{\mathrm{HCl}})$ which are the potential curves of the molecule, we took the values calculated by Bettendorff *et al.*,[45] who used a very accurate *ab initio* approach.

For V_{ArAr} in Eq. (4), representing the interactions between the Ar atoms, we used a sum of pairwise potentials,

$$V_{\mathrm{ArAr}}(\mathbf{R}_1,\ldots,\mathbf{R}_N)=\sum_{i>j} U_{\mathrm{ArAr}}(R_{ij}), \tag{5}$$

where $R_{ij}=|\mathbf{R}_i-\mathbf{R}_j|$. For $U_{\mathrm{ArAr}}(R)$, the Ar-Ar pair interaction, we used the potential of Aziz and Slaman.[46] For V_{HAr}, the interaction between the hydrogen and the Ar atoms, a sum of pair interactions was used:

$$V_{\mathrm{HAr}}(\mathbf{R}_{\mathrm{H}},\mathbf{R}_1,\ldots,\mathbf{R}_N)=\sum_{i=1}^{N} U_{\mathrm{HAr}}(|\mathbf{R}_{\mathrm{H}}-\mathbf{R}_i|). \tag{6}$$

For $U_{\mathrm{HAr}}(R_{\mathrm{HAr}})$ we used a Lennard–Jones function fitted to the H-Ar potential of Bickes *et al.*[47] Consider next the term V_{ClAr} in Eq.(4): Also this is taken to be a sum of pairwise Cl-Ar interactions:

$$V_{\mathrm{ClAr}}(\gamma,\mathbf{R}_{\mathrm{Cl}},\mathbf{R}_1,\ldots,\mathbf{R}_N)=\sum_{i=1}^{N} U_{\mathrm{ClAr}}(\gamma,R_{i\mathrm{Cl}}), \tag{7}$$

where $R_{i\mathrm{Cl}}=|\mathbf{R}_i-\mathbf{R}_{\mathrm{Cl}}|$. Models for such interactions were extensively pursued in the context of P-state atom dynamics in rare-gas hosts.[40–43] A very satisfactory empirical description is obtained by models that include not only the dependence of the interaction on the Ar-Cl distance, but also a dependence on the *orientation* of the p-orbital of the Cl with respect to the Cl-Ar axis. The anisotropy of the P-state atom interactions turns out to be of crucial importance in governing the dynamics of the systems involved.[40–43] Such an accurate Cl-Ar anisotropic interaction was determined by Aquilanti and coworkers,[48] and employed here, as well in a previous study on Cl atoms in solid Ar.[42] It has the form

$$U_{\mathrm{ClAr}}(\gamma,R_{\mathrm{ClAr}})=U^{(0)}_{\mathrm{ClAr}}(R_{\mathrm{ClAr}})+U^{(2)}_{\mathrm{ClAr}}(R_{\mathrm{ClAr}})P_2(\cos\gamma), \tag{8}$$

where γ is an electronic coordinate, representing the angle between the orientation of the p orbital of the Cl and the Cl-Ar axis. The orientation angle γ is thus, within the DIM model, the only electronic degree of freedom in Eq. (7). $U^{(j)}_{\mathrm{ClAr}}(R_{\mathrm{ClAr}})$ are functions of the Cl-Ar distance only, and are given in Ref. 48. Finally, the spin-orbit coupling operator in Eq. (4) is given by

$$\hat{V}_{\mathrm{SO}}=\Delta\sum_{i=1}^{2}\hat{l}_i\hat{s}_i, \tag{9}$$

where $\hat{l}_i$ and $\hat{s}_i$ are the orbital angular momentum and spin operators of electron i, and the summation is over the two electrons included in this model. For Δ we took the spin-orbit splitting parameter of an isolated $\mathrm{Cl}(^2P)$ atom (0.109 eV), that should provide a good approximation.

The adiabatic potential energy surfaces of the system, $W_n(\mathbf{R})$, are given by solution of the (electronic) Schrödinger equation:

$$H_{\mathrm{el}}(\gamma,\mathbf{R})\,\phi_n(\gamma,\mathbf{R})=W_n(\mathbf{R})\,\phi_n(\gamma,\mathbf{R}). \tag{10}$$

Thus, to obtain the $W_n(\mathbf{R})$, the Hamiltonian $H_{\mathrm{el}}(\gamma,\mathbf{R})$ of Eq. (4) is diagonalized in the Valence-Bond basis, Eqs. (1)–(3), at each configuration $\mathbf{R}$ of interest, where $\mathbf{R}$ represents the position of all the nuclei in the system. As we shall describe below, the determination of the $W_n(\mathbf{R})$ is actually done ''on the fly,'' along computed trajectories for the dynamics.

B. Surface-hopping molecular dynamics simulations

The non-adiabatic processes were simulated in this study by a semiclassical surface hopping algorithm, similar to the version proposed by Tully.[49] Evidence from applications to processes related to the one studied here, e.g. electronic relaxation of P-state atoms in solids and in clusters,[40–43] supports the validity of the method at least on a semiquantitative footing. The accuracy of the method for large systems, as studied here, is however still not known. A recent study for $(\mathrm{Ar})_{10}\mathrm{Ba}$, $(\mathrm{Ar})_{20}\mathrm{Ba}$, using a more accurate method that treats both electronic and nuclear degrees of freedom quantum mechanically, shows that the method is valid for many properties, but also that it can be in significant error, e.g., for the populations of some of the electronic states.[50] However, the quantum mechanical simulations are not yet feasible for systems as large as the one studied here, and our impression is that the Tully method is at least as satisfactory as any of the alternative, practical approximations for extended systems. We give here a brief outline of the algorithm, following the

version used in Refs. 42 and 43. In this method, nuclear motions are treated by classical dynamics. Suppose that initially the system is on one of the adiabatic potential energy surfaces $W_n(\mathbf{R})$, where $\mathbf{R}$ denotes the positions of all the nuclei. As long as non-adiabatic transitions do not occur, the atoms are propagated by a classical trajectory on that surface. At any point in time along the trajectory, one can compute the adiabatic potential surfaces $W_j(\mathbf{R})$ (of which there are 12 in the present case), and the corresponding adiabatic electronic states $\phi_j(\gamma,\mathbf{R})$ where γ is the electronic degree of freedom pertaining to the orientation of the p-orbital. This is done ''on the fly'' by diagonalizing the electronic Hamiltonian of Eqs. (4)–(9), in the ''Valence Bond'' basis of Eqs. (1)–(3). The diagonalization yields uniquely the eigenvalues $W_j(\mathbf{R})$ at each configuration $\mathbf{R}$ of the nuclei. Note, however, that the electronic eigenfunctions $\phi_j(\gamma,\mathbf{R})$ are *not* uniquely determined by the diagonalization. If the $W_j(\mathbf{R})$ are not exactly degenerate at $\mathbf{R}$, then $\phi_j(\gamma,\mathbf{R})$ is ambiguous within an $\mathbf{R}$-dependent phase factor $\exp(i\lambda(\mathbf{R}))$, where $\lambda(\mathbf{R})$ is a real-valued function. In such cases, and if the Hamiltonian includes only real-valued scalar potential functions, the adiabatic states can be chosen to be real-valued, and the algorithm for calculating the non-adiabatic transitions is well-defined and valid.[42,51,52] In cases where exact degeneracy occurs, the ambiguity in determining the $\phi_j(\gamma,\mathbf{R})$ by diagonalization poses a much more complicated problem, and a much more elaborate algorithm is necessary to overcome the difficulty. An example is a $\mathrm{Cl}(^2P)$ atom in a rare-gas environment, where the two-fold Kramers degeneracy occurs.[42] In present case there is no permanent degeneracy, however, due to spin-orbit coupling the adiabatic states *cannot* be chosen real-valued. Here we apply gauge constrain similar to one described in Ref. 42: phases of $\phi_i(\gamma,\mathbf{R})$ were chosen to minimize deviation of the adiabatic states from reference ones:

$$\lambda_i(\mathbf{R}) = \arg\min_{\lambda_i} \left| |\Phi_i\rangle - e^{-i\lambda_i(\mathbf{R})} |\phi_i(\gamma,\mathbf{R})\rangle \right|, \tag{11}$$

where $\Phi_i \equiv \phi_i(\gamma,\mathbf{R_0})$ is the reference state being the adiabatic state at a fixed configuration $\mathbf{R}_0$. Note that the phase of Φ_i is fixed. From Eq. (11) one obtains: $\lambda_i = \lambda_i^1$, where $\langle\phi_i(\gamma,\mathbf{R})|\Phi_i\rangle = |\langle\phi_i(\gamma,\mathbf{R})|\Phi_i\rangle| e^{i\lambda_i^1}$, which is equivalent to the gauge:[51]

$$\mathrm{Im}\langle\Phi_i|\phi_i(\gamma,\mathbf{R})\rangle = 0, \quad \langle\Phi_i|\phi_i(\gamma,\mathbf{R})\rangle > 0. \tag{12}$$

Since the adiabatic electronic states are generated ''on the fly'' along a trajectory $\mathbf{R}(t)$, we can write $\phi_j(\gamma,\mathbf{R}) \equiv \phi_j(\gamma,t)$ for that trajectory. In the semiclassical surface hopping method, the electronic degree of freedom is described by a wavefunction $\psi(\gamma,t)$, that evolves in time according to the Schrödinger equation:

$$i\hbar \frac{\partial\psi(\gamma,t)}{\partial t} = H_{\mathrm{el}}(\gamma,\mathbf{R}(t))\,\psi(\gamma,t), \tag{13}$$

where $H_{\mathrm{el}}(\gamma,\mathbf{R}(t))$ is the electronic Hamiltonian given by Eqs. (4)–(9), with the trajectory function substituted for the nuclear positions $\mathbf{R}$. We expand the electronic wavefunction $\psi(\gamma,t)$ in the adiabatic basis $\phi_j(\gamma,t)$:

$$\psi(\gamma,t) = \sum_{j=1}^{12} C_j(t)\,\phi_j(\gamma,t). \tag{14}$$

This leads to the following equations for the coefficients $C_j(t)$, as given by Tully:[49]

$$i\hbar\dot{C}_k(t) = -i\hbar\sum_j C_j(t)\langle\phi_k|\dot{\phi}_j\rangle_\gamma + \sum_j C_j(t)W_j(\mathbf{R}(t)). \tag{15}$$

Using the properties of the adiabatic eigenstates, we get:

$$\langle\phi_k(\gamma,\mathbf{R})|\nabla_R\phi_j(\gamma,\mathbf{R})\rangle_\gamma = \frac{\langle\phi_k(\gamma,\mathbf{R})|\nabla_R H_{\mathrm{el}}(\gamma,\mathbf{R})|\phi_j(\gamma,\mathbf{R})\rangle_\gamma}{W_j(\mathbf{R}) - W_k(\mathbf{R})}. \tag{16}$$

Variation of normalization condition yields that the real parts of diagonal matrix elements are equal to zero, however imaginary parts can be non-zero. Expressions for them are derived in:[51]

$$\langle\phi_k(\gamma,\mathbf{R})|\nabla_R\phi_k(\gamma,\mathbf{R})\rangle_\gamma = -\frac{i}{\langle\Phi_k|\phi_k(\gamma,\mathbf{R})\rangle_\gamma}\mathrm{Im}\left[\sum_{l\neq k}\frac{\langle\Phi_k|\phi_l(\gamma,\mathbf{R})\rangle_\gamma\langle\phi_l(\gamma,\mathbf{R})|\nabla_R H_{\mathrm{el}}(\gamma,\mathbf{R})\phi_k(\gamma,\mathbf{R})\rangle_\gamma}{W_k(\mathbf{R}) - W_l(\mathbf{R})}\right]. \tag{17}$$

Using the classical motion of the nuclear coordinates $\mathbf{R}$, the left hand side of Eqs. (16), (17) can be written

$$\left\langle \phi_k \middle| \frac{\partial\phi_j}{\partial t} \right\rangle = \dot{\mathbf{R}}(t)\langle\phi_k(\gamma,\mathbf{R})|\nabla_R\phi_j(\gamma,\mathbf{R})\rangle_\gamma, \tag{18}$$

where $\mathbf{R}$ is the velocity vector of the nuclei in the system. Eqs. (16)–(18) provide a convenient way for the calculations of the time-dependent quantities $\langle\phi_k|\dot{\phi}_j\rangle_\gamma$ which represent the non-adiabatic coupling. These also are computed ''on the fly'' with the propagation of the trajectory $\mathbf{R}(t)$.

The classical propagation of the nuclei, together with Eqs. (12),(14)–(18) for the time-dependent electronic wavefunction and for the non-adiabatic couplings between the $\phi_j(\gamma,t)$, are the basis of the ''surface hopping'' algorithm. Suppose that initially, at $t=t_0$, $C_j(t_0)=1$, $C_k(t_0)=0$ for $k \neq j$. The nuclei are then propagated on the adiabatic surface $W_j(\mathbf{R})$. At each point along the trajectory the 12 adiabatic potentials and the corresponding eigenstates are constructed, and the non-adiabatic couplings $\langle\phi_k|\dot{\phi}_j\rangle_\gamma$ are obtained. Eqs.(15) for the coefficients $C_k(t)$, $k=1,\ldots,12$ are solved

numerically and their variation in time is followed. At sufficiently small time intervals, we test for the occurrence of a ''surface hopping'' event: $|C_k|$ is compared with a generated random number λ, $0 \leqslant \lambda < 1$, and on the basis of this stochastic criterion it is decided whether a ''hop'' from surface j to surface k has taken place or not. For stability of the results it was necessary to test for the possible occurrence of hopping each 50 integration steps. This procedure, used by us also in Refs. 42,43 differs from the ''minimum number of hops'' criterion employed by Tully,[49] but our tests for several systems suggest that in general the two algorithms should give similar results. Once a hopping event has occurred, at some $t=t_1$, we reset the values of the coefficients: $C_k(t_1)=1$, $C_l(t_1)=0$ for $l \neq k$. The procedure is then continued with the nuclei being propagated on the surface $W_k(\mathbf{R})$. The initial values for the propagation of the trajectory on the new surface are very similar to those discussed by Tully.[49]

C. The simulations

As the first step in the calculations, the system of 255 Ar atoms and a single HCl molecule (with periodic boundary conditions at the ends) was equilibrated in the electronic ground state at 17 K. This equilibration was carried out by a long ($\sim$20 ps) trajectory run, following standard prescriptions of Molecular Dynamics simulations.[53] At random times after equilibration, ''snapshots'' of the system (nuclear configurations, momenta) were recorded. The overall rotational and vibrational distributions on the ground state were analyzed: we found that HCl rotates almost freely in Ar lattice at temperature used in our simulations. It results in uniform rotational distribution, which is in a good agreement with quantum mechanical study of Schmidt and Jungwirth.[54] The vibrational coordinate distribution of the HCl internal mode is very different from quantum one due to high frequency of HCl vibrations. However, the effect of this on photodissociation is small. This is especially the case for fixed excitation energy and a narrow excitation window, which wash out the difference almost completely.

For each of these configurations, electronic excitation was modeled in the spirit of the classical limit of the Franck-Condon Principle: The system was promoted vertically by a given excitation energy, retaining the positions and momenta of all the nuclei upon excitation. The excitation energy we used was 7.22 eV, well within the observed absorption band of gas-phase HCl.[13] With this energy, each excitation event is found to land on one of the two lowest adiabatic potential surfaces of the system. In fact the population produced in the two states by all the excitation events is about equal. Projection of the two lowest adiabatic states onto the ''bare'' molecular states shows that in effect only the $^3\Pi_0$ states of the HCl was selected by the excitation wavelength used. Our motivation to study photodynamics following excitation to triplet Π state was to study the process on the *lowest* excited state of HCl. In this situation we expected that cage exit will be relatively slow (due to low excess energy). A comment should be made on the possibility of exciting HCl to the triplet Π state experimentally: In one-photon experiments it is probably impossible to distinguish absorption to triplet Π state (allowed due to interaction with a matrix) from absorption by the singlet Π state, because both these wide transitions overlap, and because the transition dipole moment is weaker, though not zero, for the excitation to the triplet. Therefore such an experiment is impossible in a one-photon framework. However, triplet states can be selectively excited in multi-photon experiments with suitable phase combination of excitation photons.

After excitation into an excited adiabatic state, the system was propagated according to the simulation method described earlier, including occasionally non-adiabatic transition events. Although in the Franck-Condon region only two adiabatic states can be accessed with the excited energy used, away from the Franck-Condon region the gaps between several of the potential surfaces become smaller, in some cases intersect, and more adiabatic states can be reached in the course of the dynamics. Each trajectory was propagated for several picoseconds following the excitation event. A total of 105 excitation trajectories was run.

We analyzed the statistical error introduced by the finite size of the statistical ensemble using a binomial distribution. For the observables which are averaged over all electronic states, 105 trajectories yield a relatively small uncertainty. F.i., statistical error for observed recombination yield is about 4%. However, for state-dependent observables (as branching ratios for distinct states) the statistical uncertainty is much larger which is shown by large error bars in Figs. 17, 18.

III. RESULTS AND DISCUSSION

It will be convenient to organize the presentation of the results around several of the main findings.

A. Time-dependence of cage exit and of recombination

We considered as a cage-exit event in the simulations a situation in which the H atom reached a distance of half a lattice constant or more from the (substitutional) site of the HCl center of mass prior to photoexcitation. While the definition is somewhat arbitrary, the results obtained are such as to be robust with regard to minor changes in the definition. We note that in none of the trajectories did we have a ''recrossing'' behavior: The H atom leaving the cage according to the above definition, then returning later on. In principle, of course, such recrossings may take place. In the trajectories where the H atoms exited the original cage, they were found to ultimately reach an octahedral-interstitial site. This was found to be the case also in earlier simulations on the photolysis of HI in solid Xe,[25] at least for relatively low photoexcitation energies. It is possible that at much higher photon energies, less favorable sites such as the tetrahedral-interstitial site are also populated. We counted as a *recombination* event one in which the HCl molecule has reached the ground electronic state *and* in addition the kinetic energy of the H atom has decreased to a value well less than the gap between the ground adiabatic electronic state and the first

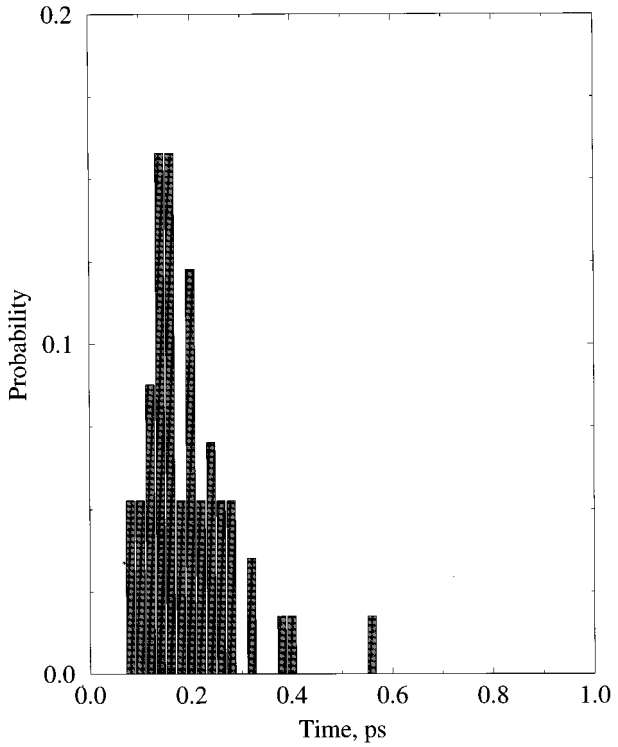

FIG. 2. Number of cage-exit events versus time.

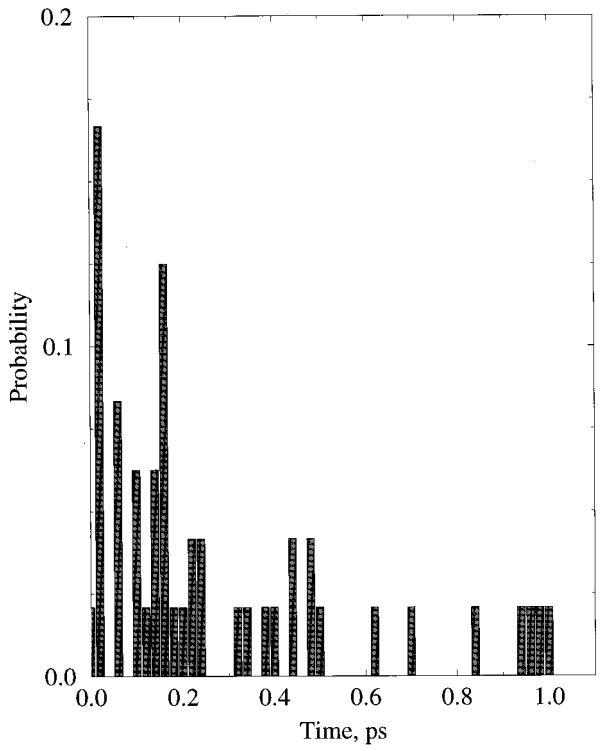

FIG. 3. Number of of recombination events versus time.

excited adiabatic state. The total energy of the system is, of course, conserved and in principle the system may cross back after recombination has occurred to an excited electronic state, according to the above criterion. However, such a fluctuation requires highly coherent motion of all atoms and, therefore, is of low probability. In the simulations this did not happen. Figure 2 shows in histograms the number of cage exit events and Fig. 3 shows the number of recombination events. Despite the limitations of the trajectory statistics, *it is evident that recombination events occur over a much larger time range then cage exit events*. The earliest recombination events occur about 15–20 fs after excitation, and recombination events keep occurring well beyond 1 ps later. The earliest cage exit events occur about 70 fs after excitation, and are thus significantly delayed. The main cage exit events occur, however, in the range of 0.15 ps to 0.25 ps after the excitation, and beyond about 0.55 ps no more cage-exit events are found.

The distribution in time of cage-exit events is simple to interpret. Almost free rotations of HCl molecule makes a direct exit hardly probable: In all the trajectories the initial impact of the H atom on the surrounding cage is such that it hits a steeply repulsive potential wall due to the Ar atom and recoils. None of the trajectories sampled lead in the first collision to the ''window,'' or transition state, where the barrier for cage exit by the H atom is sufficiently low. However, this result may be influenced by minor changes in H-Ar interaction potential: A slightly less repulsive potential can increase the size of exit windows and yield some measure of direct events. It turns out that energy transfer in the first few collisions between the H atom and the surrounding cage leads to some expansion of the cage and to widening of the cage exit ''windows.'' One of the following impacts of the H atom lands on the favorable windows, and then cage exit occurs. As found already in Ref. 25 in simulations of the photolysis of HI in solid Xe, the H atom can ''rattle'' quite a few times between the cage walls, before reaching a possible cage exit ''window.'' Figure 4 shows the path of the H atom in a trajectory that leads to relatively early cage exit, at around 70 fs. (The figure shows the projection of the three-dimensional path onto the X,Z plane of the crystal.) Also the path of the Cl atom in that trajectory is shown. The cage exit in this case was clearly delayed, following some ''rattling'' of the H atom in the cage, till the exit window was reached. Figure 5 shows the paths of the H and the Cl atoms in a trajectory that leads to cage exit after 550 fs, which corresponds to one of the longest delays found in this system.

Cage-exit event are peaked, however, at much shorter times, $t \approx 150$ fs, and the time-distribution is quite narrow. The more collision the H atom undergoes in the cage, the greater is its kinetic energy loss. After some rattling between the walls of the cage, when the kinetic energy of the H atom has fallen below the barrier for cage exit, it is bound to remain in the cage. Consider now the time-distribution of recombination events, shown in the Fig. 3. Some recombination events occur already for times only 15–20 fs after excitation. The mechanism for the very early recombination events is as follows: The H atom moves, upon excitation with great impulse and strikes an Ar atom far away from the Cl. At this point the H atom has no or little kinetic energy,

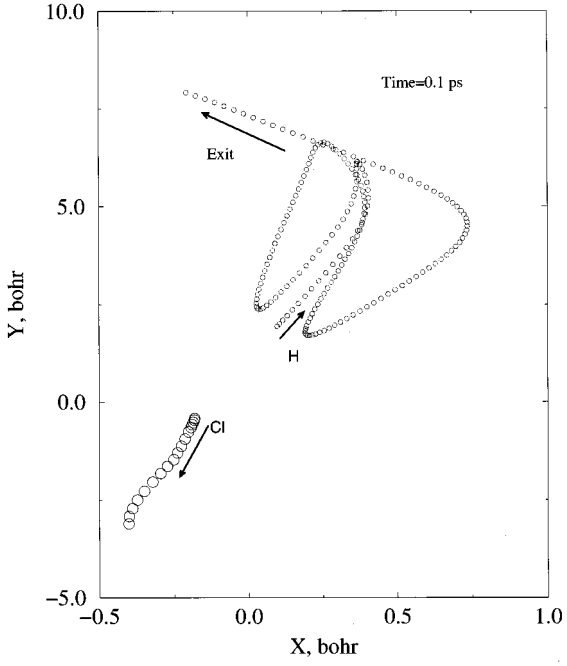

FIG. 4. The paths of the H and the Cl atoms in a trajectory leading to early cage exit (after 0.07 ps). X and Z are two axes defining a crystal plane, onto which the path is projected.

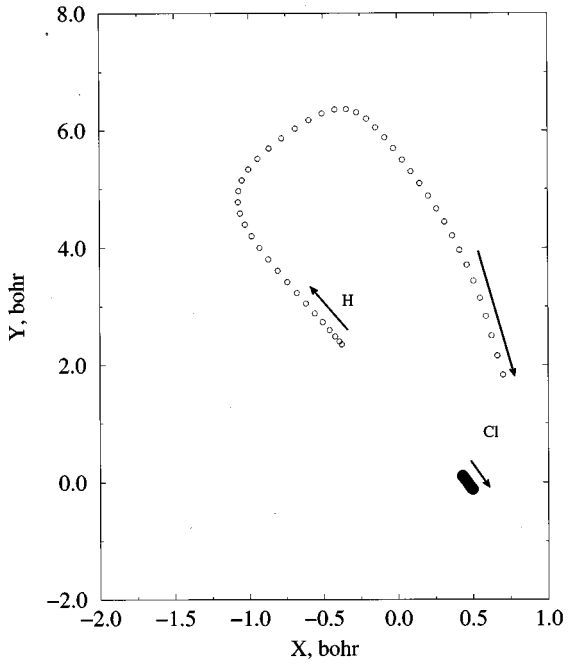

FIG. 6. The paths of the H and of the Cl atoms in a trajectory leading to fast recombination (after 0.02 ps).

but has high potential energy. Some of the configurations where the Cl atom and the H atom are mutually quite far (although within the cage) are favorable for transition into the ground electronic state, since the excited adiabatic potential surface crosses with the ground state surface, or approaches the latter very closely, for some such configurations. The fact that the H atom has little velocity at this point is favorable for the transition, since it implies that the hydrogen remains at the vicinity of that configuration at least for some brief time interval, over which the nonadiabatic transition can occur. After the electronic transition, the H atom is accelerated over the ground-state adiabatic potential energy surface, gaining kinetic energy that it later loses by collisions to the Cl and the Ar atoms. The system remains, however, in the ground state. Figure 6 shows the path of the H and Cl atoms in a trajectory that leads to very early recombination—basically a single excursion of the H atom to the cage wall has sufficed for the occurrence of the process. Unlike the above direct nonadiabatic crossing to the ground state, there are many events in which the system carries out many nonadiabatic transitions, cascading down the manifold of potential energy surfaces, until ultimately it reaches the electronic ground state. In fact, in all cases where the hydrogen has lost already the kinetic energy amount necessary for it to overcome the cage-exit barrier, relaxation onto the ground electronic state and recombination onto it are bound to happen—yet the process may take some time, well beyond 1 ps. Figure 7 shows the paths of the H and of the Cl atoms in a trajectory in which the point of recombination on the ground state is reached 1.4 ps after the excitation. In this trajectory the H atom collided 20 times with the cage walls before recombination. It turns out that already 0.5 ps after excitation the H atom was already cold to the point of excluding cage exit. However, the nonadiabatic electronic transitions all the way to the ground state took a much longer time to occur. The results of the simulations and the view afforded on the

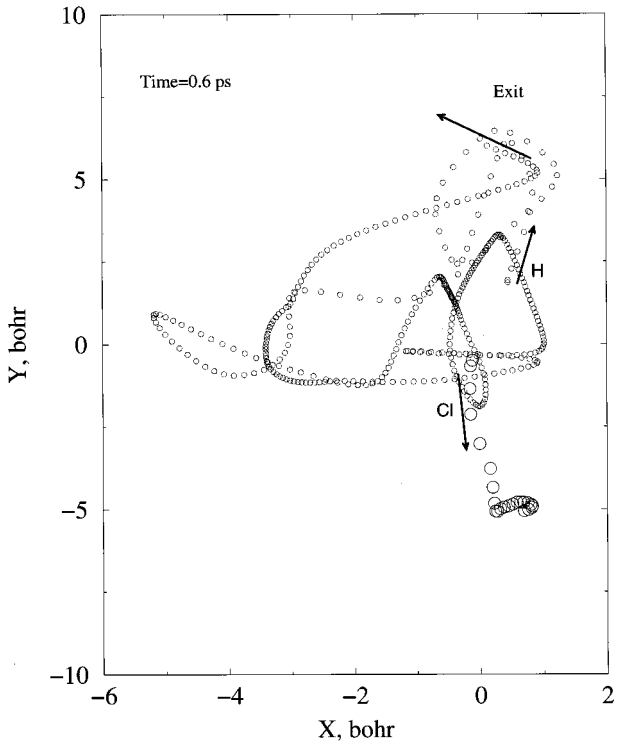

FIG. 5. The paths of the H and of the Cl atom in a trajectory leading to very delayed cage exit (after 0.55 ps).

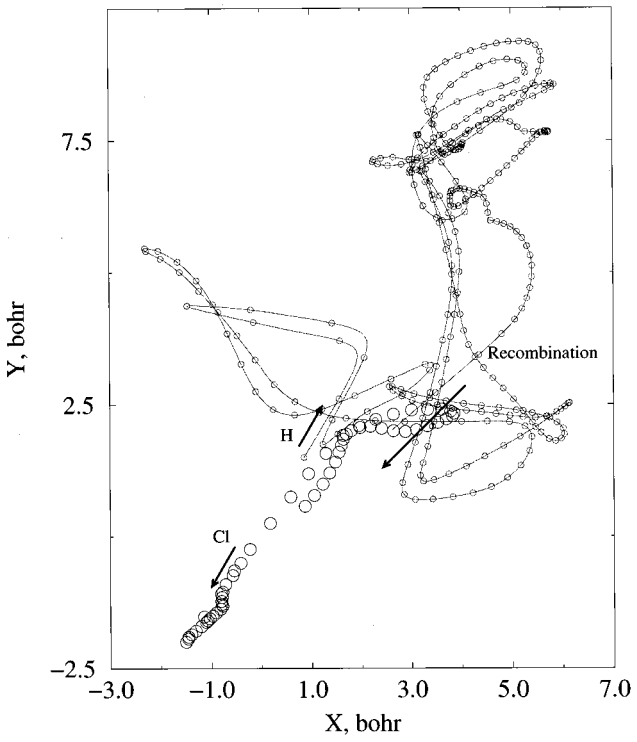

FIG. 7. The paths of the H and of the Cl atoms in a trajectory ending in very delayed recombination (after 1.4 ps).

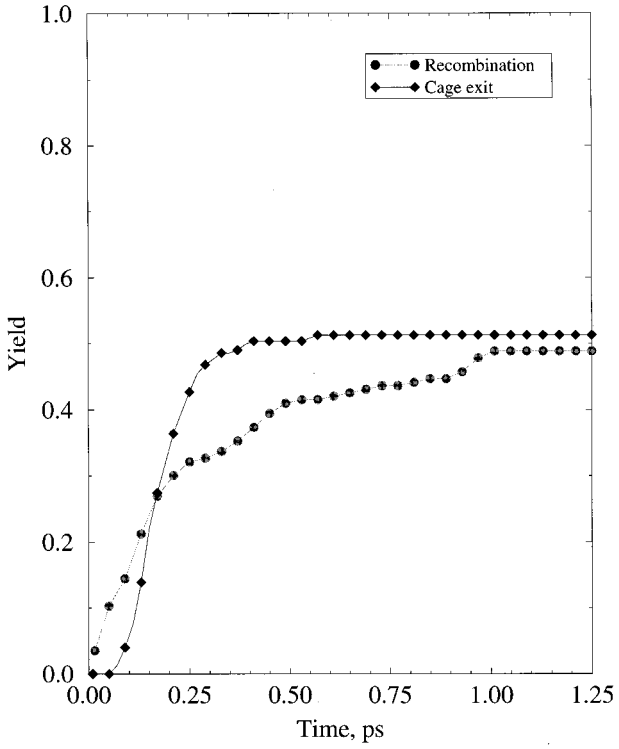

FIG. 8. The yields for cage exit and for recombination as a function of time after the excitation pulse.

dynamics in time of the cage exit and recombination events, depend of course on the interaction potential. It is possible that the ''real'' H-Ar potential, for instance, is less repulsive than the one we used. It is conceivable that in this case there will be much less delay of cage-exit, perhaps some measure of *direct* cage exit will take place. We estimate, however, on the basis of the trajectories we examined that no *realistic* H-Ar potential is likely to change the fact of *at least* an important component of delayed cage exit events. We believe this conclusion is likely to remain robust, regardless of the uncertainty, important as it is, as to the accuracy of the potentials.

B. Yields for cage exit and for recombination

The yield for cage exit at time t after the excitation pulse is given by: $Y_{\mathrm{ex}}(t)=\int_o^t p_{\mathrm{ex}}(t\prime)dt\prime$, where $p_{\mathrm{ex}}(t')$ is the probability per unit time for cage exit. $Y_{\mathrm{rec}}(t)$, the yield for recombination, is similarly defined. The yields for cage exit and for recombination as a function of time are shown in Fig. 8. The yields for the two processes are roughly of similar magnitude for $t\gtrsim 1$ ps, with Y_{ex} somewhat larger than Y_{rec}. The asymptotic long-time ratio between the yields is 54:46($\pm$4.5%). It is interesting to compare this result with a recent experiment: Schwentner and coworkers[14] observed 30%–40% dissociation efficiency with uncertainty of 30% at the excitation of 7.2 eV. Therefore, the calculated and observed photodissociation yield are in good agreement. However, the comparison must be treated with caution, since in the simulation the initial excited state was the triplet only.

Because of the delayed nature of cage exit in this process, while some recombination events take place shortly after the excitation, $Y_{\mathrm{rec}}(t)$ is larger than $Y_{\mathrm{ex}}(t)$ for very short times, the crossover point being around 0.125 ps. The results should depend on the excitation energy, and one expects that for higher excitation energies the ratio of Y_{ex} to Y_{rec} will be larger. Accurate measurements of the two yields should be of great interest.

C. Cage exit and cooling mechanism for the H atom

The excitation energy used in the simulations corresponds to an excess energy of 2.5 eV (in gas phase photodissociation). Due to the mass ratio between H and Cl, almost the entire excitation energy is converted into kinetic energy of the hydrogen. The energy suffices, in principle, for yielding a hot distribution for the H atoms after cage exit. In fact, the simulations show that the kinetic energy of the H atoms right after cage exit is not very high. The kinetic energy distribution immediately after cage exit is shown in Fig. 9. The hottest H atoms have kinetic energies of $\sim$0.5 eV only at cage exit, and the maximum of the distribution is at about half this energy value only. Figure 10 shows the kinetic energy of the H atom in a trajectory leading to relatively fast cage exit. In the upper part of the figure, the kinetic energy along the trajectory is compared with results of a model assuming hard-sphere collisions between the H and isolated Ar or Cl atoms. The lower figure shows the H-Cl distance versus time, and this provides also the collision times (the maxima of $R_{\mathrm{H-Cl}}$ correspond to H-Ar collisions,

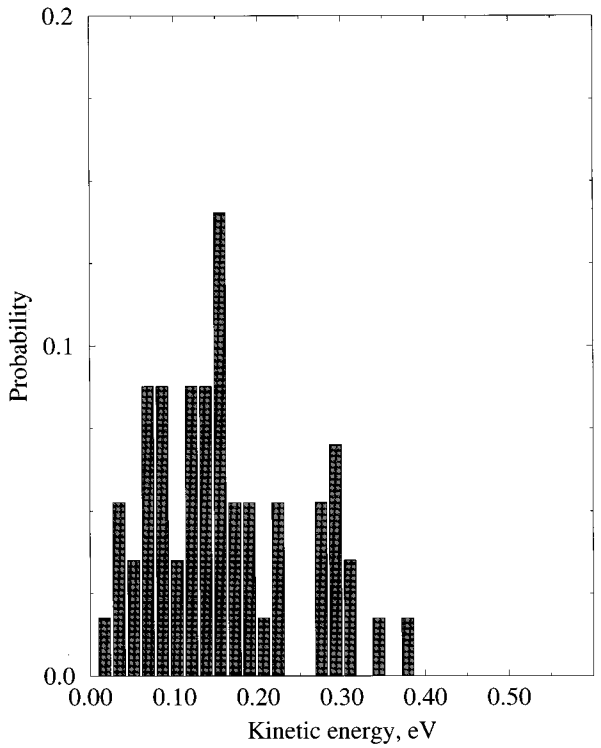

FIG. 9. Kinetic energy distribution of H atoms immediately after cage exit.

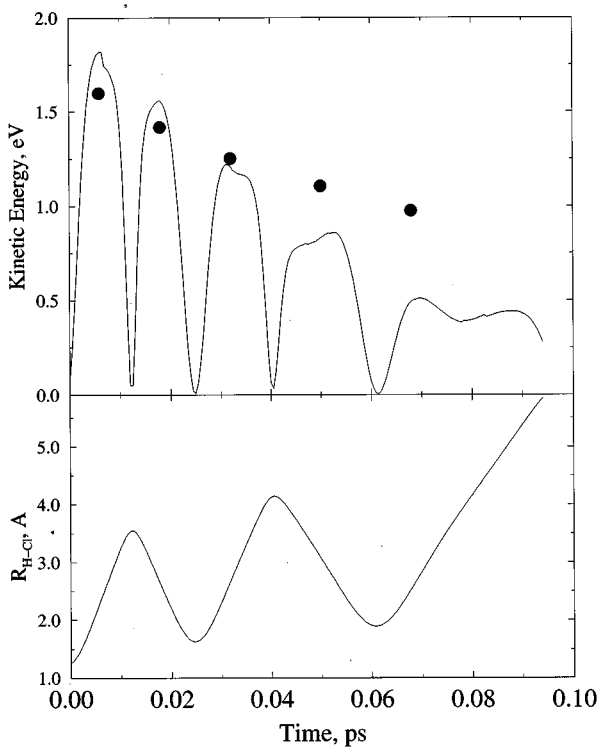

FIG. 10. Upper part: Kinetic energy of the H atom versus time in a particular trajectory resulting in fast cage exit (solid line). The black dots give the kinetic energy from a ''hard-sphere'' collision model between the H atom and Ar or Cl. Bottom part: The H-Cl distance versus time in the same trajectory.

the minima correspond to H-Cl encounters). The number and times of collisions from the bottom of Fig. 10 were used in the simple ''hard-sphere collisions'' calculation. We note that by Fig. 10, the cooling of the H by the Ar lattice is more efficient than that by isolated hard sphere collisions, especially for longer times. It seems that as the H atom slows down, it can interact with collective modes of the solid, transferring energy more effectively. Also, at least for slower hydrogen, longer ranges of the H-Ar interaction play a role not included, of course, in the hard sphere model, making the cooling more efficient.

D. Electronic transitions in cage exit and in recombination

We consider now the trajectory corresponding to the fastest cage exit event. The upper part of Fig. 11 shows the H-Cl distance versus time for that trajectory. The middle panel shows the adiabatic potential energy surfaces along the trajectory, and the bottom figure gives the electronic state of the system as a function of time. (The numbers of the electronic states of the system, from 1–12, correspond to the ordering of the states as described in Sec. II.) For this particular trajectory cage exit occurs after two collisions with the cage walls (and two collisions with the Cl atom). As seen from Fig. 11(c), *the electronic state changes already in the first collision, and cage exit does not occur from the initial state*. In fact, there are over 15 nonadiabatic transitions along that trajectory, mostly during the two collisions with the Ar atoms, although during each collision several nonadiabatic transitions take place. Actually, several nonadiabatic transitions take place during the cage-exit stage itself. We conclude that *nonadiabatic transitions may occur even in the fastest cage exit events, and indeed they play a major role in the detailed dynamics of the cage exit event*. As Fig. 11(b) shows, the nonadiabatic transitions occur when the relevant adiabatic potential energy surfaces cross, or approach very closely (we show only some of the potential energy surfaces, for clarity). In many cases these crossings or near crossings arise when the Cl atom is relatively far from the hydrogen (this reflects on the degeneracies and the small splittings between $Cl(^2P)$ atom states in a matrix, when no H atom is present). Figure 12 shows the most delayed cage-exit trajectory. In this case the H atom leaves the cage after 9 collisions with the cage walls. The number of nonadiabatic transitions throughout this event is very large, as seen in Fig. 12(c). In fact, throughout the process, the system goes through all the 12 electronic states of the manifold. Very interestingly, during the trajectory the system reaches twice the ground electronic state, but the kinetic energy of the H atom has remained sufficiently high, leading to back transitions to the excited adiabatic potential surfaces, and ultimately to cage exit. Thus, *return to the electronic ground state during the process is not a sufficient condition for recombination.* Also, as we saw, *nonadiabatic transitions are important for both fast and slow cage exit events, but in fast cage-exit events the system only reaches a few of the excited potential energy*

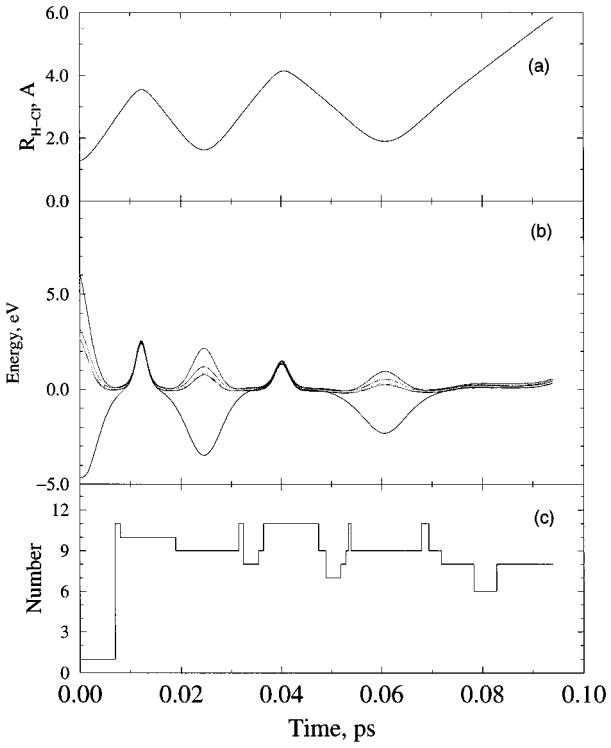

FIG. 11. Electronic transitions in a trajectory leading to the fastest cage exit. (a) The H-Cl distance versus time in the trajectory. (b) Adiabatic potential energy surfaces along the trajectory. (c) The electronic state of the system versus time. The states are numbered from 0–11, $n=0$ is the ground state and $n=1,2$ are the states of initial excitation. Higher n corresponds to the higher energy.

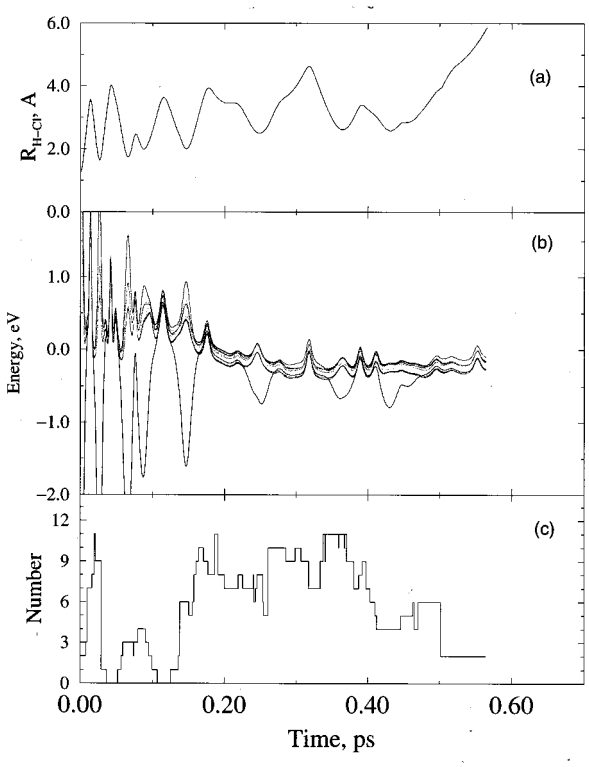

FIG. 12. Electronic transitions in a trajectory leading to the slowest observed cage exit. (a) The H-Cl distance versus time. (b) Adiabatic potential energy surfaces along the trajectory. (c) The electronic state of the system at each time. For numbering of states, see Fig. 11, and Sec. II.

surfaces, while in a very delayed cage exit it may go through all the electronic states of the manifold involved, including the ground state.

We consider now electronic transitions during recombination events. Figure 13 corresponds to the fastest recombination event seen in the simulation, in which the hydrogen undergoes only a single collision with the cage walls. *As this figure shows, this may suffice for recombination*, but is actually not typical and most trajectories resulting in recombination involve at least two collisions with the walls. As Fig. 13 shows, the recombination occurs due to direct nonadiabatic transitions, when the H atom hits the cage wall and is far from the Cl atom. Another brief nonadiabatic event occurs during the collision: The system returns to the excited state for a very brief time interval, then goes back to the ground state. Finally, Figure 14 shows results for the most delayed recombination event we calculated. The recombination in this trajectory occurs 1.4 ps after recombination. During the process, the H atom undergoes about 20 collisions with the cage walls. Actually, after $t\approx 0.5$ ps, the H atom is in this case already too cold for cage exit. However, the system carries out a long and slow excursion in the space of electronic states. It spends most of the time in the electronic states which have the index numbers $n\geqslant 5$ (see Sec. II for the number labeling), although it also reaches the states 1–4 for a very brief time duration, hopping almost at once from state to state. The system reaches the electronic ground state only once, when recombination occurs. As Fig. 14(b) shows, during the trajectory the H atom is in regions where several (excited) electronic surfaces are very close, and thus carries out very frequent hops from state to state. Indeed, the H atom oscillates nearly all the time between the Cl atom and regions very far from it, in ''remote'' corners of the cage, near the wall. This trajectory is an example of a long excursion in a large subspace of the electronic states, with almost continuous hops from state to state.

E. Electronic state populations versus time

Figure 15 shows the populations as a function of time of the two lowest excited adiabatic states, those initially excited. It is evident that the decay is extremely fast, having essentially the timescale of the first collision of the H atom with the cage walls (about 10 fs). As we noted previously, nonadiabatic transitions, from the excited states to the ground state or to other excited states, take place with relatively high probability when the Cl atom is far from the H atom, which is the origin for the relation between the electronic population lifetimes and the occurrence of collisions, in particular the first one. As this, and the results of subsection 4 above show, nonadiabatic transitions in this system are extremely fast.

For purposes of interpretation it is convenient to consider the populations of the ''bare'' electronic states of the HCl molecule, that is the states without the effect of the environment. We stress that this can only be done as a crude

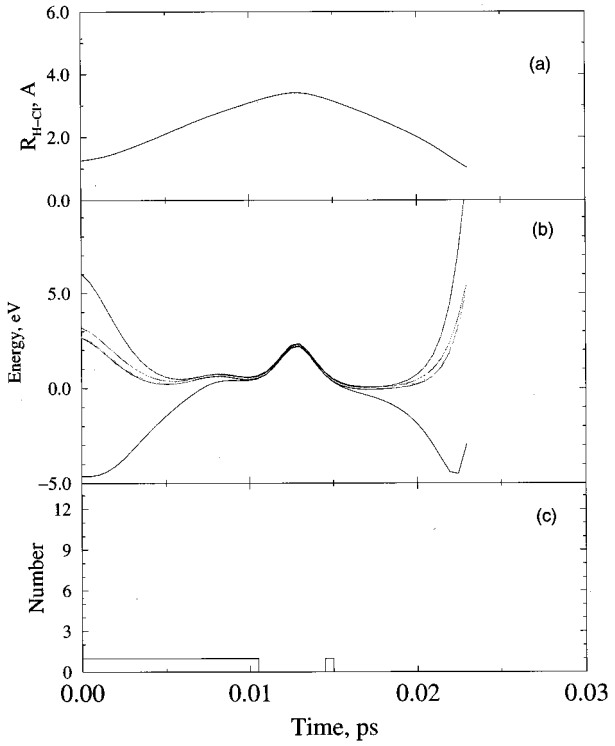

FIG. 13. Electronic transitions in a trajectory leading to the fastest recombination. (a) The H-Cl distance versus time. (b) Adiabatic potential energy surfaces along the trajectory. (c) The electronic state of the system at each time (for the state numbering, see Fig. 11, and Sec. II).

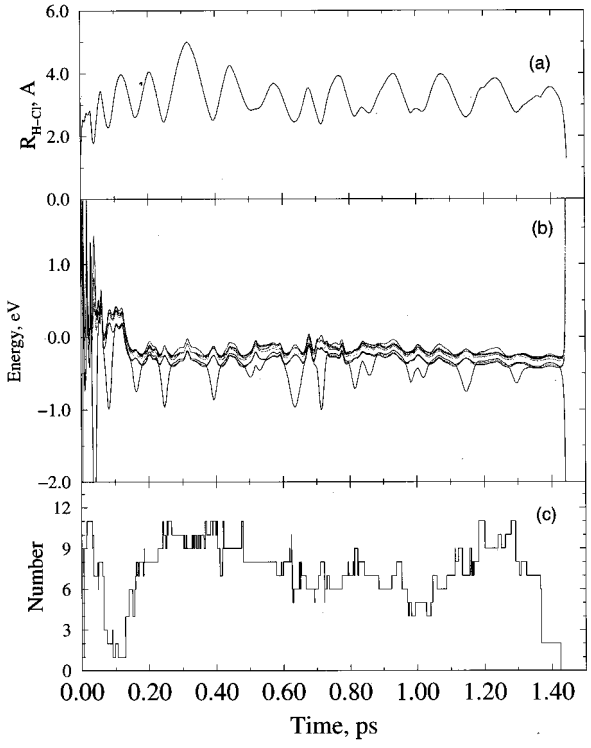

FIG. 14. Electronic transitions in a trajectory leading to the slowest recombination event. (a) The H-Cl distance versus time. (b) Adiabatic potential surfaces along the trajectory. (c) The electronic state of the system at each time (for state numbering, see Fig. 11, and Sec. II).

approximation, and not in all cases. The approach we took is to project the adiabatic state at each point along the trajectory, on the ''bare'' state of HCl. Only when a single overlap dominates strongly, can we expect the interpretation via ''bare'' states to have simple observable consequences. The reason for pursuing interpretations in terms of ''bare'' HCl states is that their symmetries provide very helpful insights. Figure 16 shows the variation in time of the ''bare'' electronic states of HCl throughout the photodissociation process. These populations were constructed on the basis of the overlap with the adiabatic states, as noted above. These electronic states must be considered to be very strongly coupled by the dynamics, since the rate of nonadiabatic transitions in the system is very high. Nevertheless, although electronic state populations can change very rapidly in time, the populations do not seem statistically distributed over the timescale shown. Partly this perhaps is due to the recombination and cage exit processes, that are still ongoing—the formation of $^1\Sigma_0$ provides a ''sink'' for the other states. In any case, neither the time behavior, nor the ratios of the populations of different states suggest that a statistical distribution has been reached. *Note for instance that the* $^3\Pi_0$ *and* $^3\Pi_2$ *states, that have very similar energies, have very different populations over the time-interval shown. This is of interest for the issue of (electronic) state selectivity in condensed phase processes.*

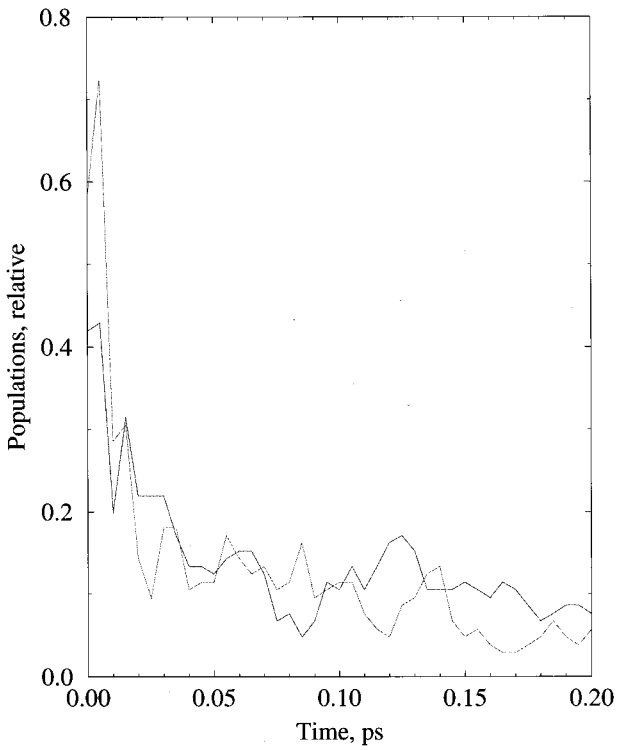

FIG. 15. The populations of the two lowest excited adiabatic states versus time. The states shown are the ones initially excited.

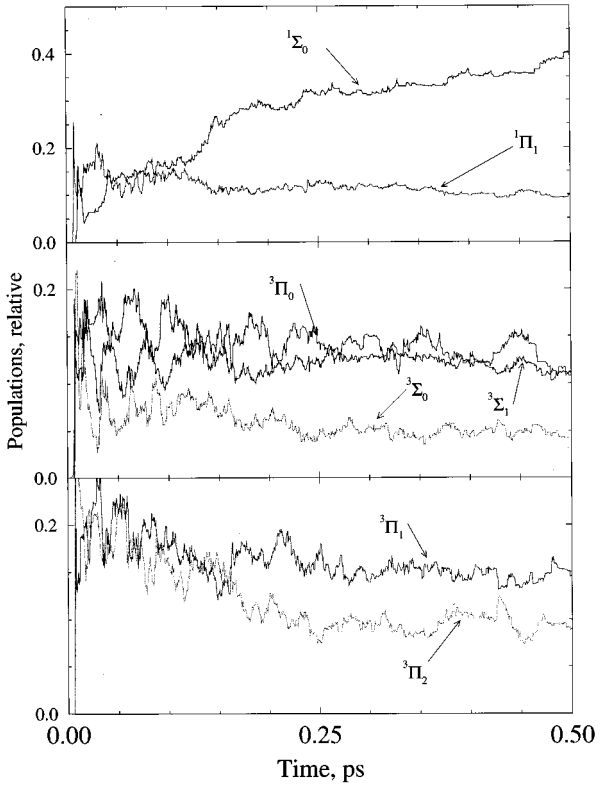

FIG. 16. The populations of the ''bare'' electronic states of HCl versus time. The populations were constructed on the basis of the project of the adiabatic states onto the bare states (see text). The relative energies of these states in an *isolated* molecule are given by Fig. 11, however in a matrix the energies of these states change due to the coupling induced by an interaction with Ar atoms.

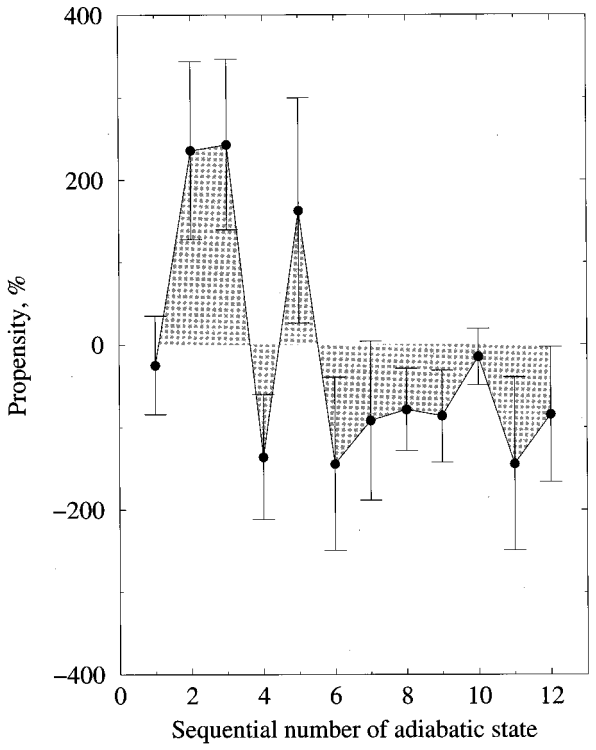

FIG. 17. $\Delta P_{\mathrm{rec-ex}}$ for the different adiabatic states. $\Delta P_{\mathrm{rec-ex}} = (P_{\mathrm{rec}} - P_{\mathrm{ex}})/P$ measures the preference for recombination over cage exit from the state. For states which favor recombination $\Delta P_{\mathrm{rec-ex}} > 0$, while states favoring cage exit have $\Delta P_{\mathrm{rec-ex}} < 0$.

F. Propensity of different electronic states with regard to cage exit versus recombination

Finally, we address the following issue: How does a given electronic state, reached by the system in a given event dictate the future evolution? Are they states of pronounced preference with regard to recombination versus cage exit? And what are the interactions or mechanisms that bring this ''preference'' about? One may expect, perhaps, since this is a system of low symmetry and very frequent nonadiabatic transitions, that significant ''preferences'' are unlikely to be found. Interestingly, this is not the case. Figure 17 shows the quantity $\Delta P_{\mathrm{rec-ex}} \equiv (P_{\mathrm{rec}} - P_{\mathrm{ex}})/P$ for the different adiabatic states. $\Delta P_{\mathrm{rec-ex}}$ is a measure of the preference for recombination as opposed to cage exit for the state. P is the average (over line) population of the state, P_{ex} is the probability of a trajectory which has reached that state to continue ultimately to cage exit, P_{rec} is the corresponding probability to proceed to recombination. We note that the average populations of most adiabatic states are about the same, which is due to the large frequency of nonadiabatic transitions in the system, and to the modest energy spacings between the excited states. Figure 17 shows only very partial correlations between the $\Delta P_{\mathrm{rec-ex}}$ and the *order* of the adiabatic states. *Since the order is approximately in accord with increasing energy of the states it is clear that energy cannot be the only or even the main factor in determining the propensity for exit versus recombination*. Note that only for the first, second and fourth excited states the propensity for recombination is greater than for cage exit ($\Delta P_{\mathrm{rec-ex}} > 0$), while for the third excited state this is not true. It is this non-monotonic behavior which indicates most strongly that in addition to energy, other factors must be important in determining the propensities of the states. Figure 18 shows $\Delta P_{\mathrm{rec-ex}}$ (defined as above) for the different ''bare'' states of the HCl molecule. The singlet $^1\Pi_1$ and the triplet Σ states ($^3\Sigma_0$ and $^3\Sigma_1$) show no preference either for recombination or for cage exit, while for $^3\Pi$ states there is a very strong dependence of $\Delta P_{\mathrm{rec-ex}}$ (the ''preference'' measure) on the projection m_j of the orbital angular momentum. The larger $|m_j|$ is, the stronger is the preference for cage exit over recombination. To understand this, consider the spin-orbit coupling between the states, and the coupling between the states due to the Ar atoms. The ground $^1\Sigma_0$ state is coupled by the interaction with the environment only to the $^1\Pi_1$ state. The spin-orbit interaction couples the ground state to $^3\Pi_0$. The latter is thus the most preferable state for recombination. The $^3\Pi_2$ state is not coupled by spin-orbit interaction to any other state. Electronic transitions from this state can only occur by coupling with $^3\Pi_0$, $^3\Sigma_1$, due to the environment. The state $^3\Pi_1$ is coupled by spin-orbit interactions to the $^1\Pi_1$ state, which in turn is coupled to the ground state by the electrostatic interaction with the Ar. This scheme of coupling, considered together with Fig. 18, leads to the following important conclu-

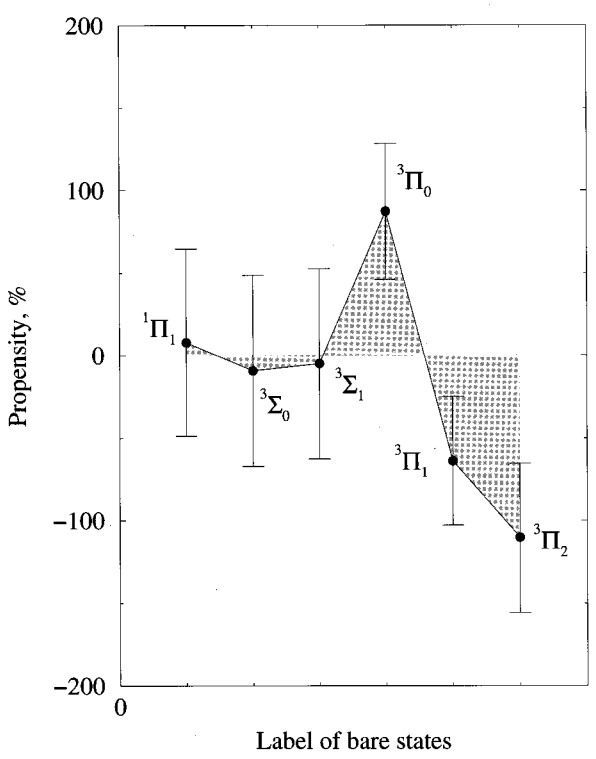

FIG. 18. $\Delta P_{\mathrm{rec-ex}}$ for the different ''bare'' states of HCl. $\Delta P_{\mathrm{rec-ex}} = (P_{\mathrm{rec}} - P_{\mathrm{ex}})/P$ measures the preference for recombination over cage exit from the state. For states which favor recombination $\Delta P_{\mathrm{rec-ex}} > 0$, while states favoring cage exit have $\Delta P_{\mathrm{rec-ex}} < 0$.

sion: *The spin-orbit interactions are the most important factor for recombination, while the interaction with the solid plays a less major role*.

IV. CONCLUDING REMARKS

In this paper we used non-adiabatic Molecular Dynamics simulations to explore cage exit, electronic transitions and recombination following photolysis of HCl in solid Ar. One of the fundamental features that emerge is the frequency, and importance, of non-adiabatic transitions between different electronic states. Such transitions were found to occur even in the fastest cage-exit events, and essentially they control much of the cage exit and recombination dynamics in time. Very rapid changes of the electronic state populations in time occur, especially immediately after photodissociation. Despite the frequent nonadiabatic transitions in this system of 12 electronic states, the populations of the states are not statistically distributed over the timescale of the process. The very interesting dynamics of the electronic states, and the behavior in time of both cage-exit and recombination events strongly underline the need for femtosecond time-resolved spectroscopic experiments to study such processes. Such experiments should open very exciting directions for comparing with theory and confirming, or rejecting, the mechanisms proposed. Of special importance would be studies of the electronic state dynamics—the variation in time of the electronic populations that clearly require ultrafast time-resolved techniques. The simulations suggest particular mechanisms for cage exit (reflected, e.g., in the time-delay predicted for these events), and for electronic transitions (many of the transitions occur when the H atom moves far away from the Cl, configurations for which the adiabatic potentials become degenerate or closely spaced). These predictions depend, however, on the validity both of the DIM potentials used, and on the surface-hopping method for the non-adiabatic dynamics. For condensed matter processes, neither of these assumptions can be taken for granted. Direct comparison between non-adiabatic Molecular Dynamics simulations and corresponding experiments for the same systems may be able to throw light on these important questions, and advance considerably our knowledge on non-adiabatic processes in condensed phases.

ACKNOWLEDGMENTS

We thank Dr. Leonid Baranov, Masha Niv, Dr. Burkhard Schmidt and Professors N. Schwentner, V. A. Apkarian, M. Chergui and V. Bondybey for helpful discussions and comments. This research was supported by a grant (to RBG) from the Israel Science Foundation (operated by the Israel Academy of Sciences). The part of this work done at UC Irvine was supported by the University Research Initiative on Advanced Cryogenic Propellants, funded by AFOSR.

[1] V.E. Bondybey and L.E. Brus, J. Chem. Phys. **62**, 620 (1975).
[2] L.E. Brus and V.E. Bondybey, J. Chem. Phys. **65**, 71 (1976).
[3] V.E. Bondybey and C. Fletcher, J. Chem. Phys. **64**, 3615 (1976).
[4] P. Beeken, M. Mandic, and G.W. Flynn, J. Chem. Phys. **76**, 5995 (1982).
[5] P. Beeken, E.A. Hanson, and G.W. Flynn, J. Chem. Phys. **78**, 5892 (1983).
[6] M.E. Fajardo and V.A. Apkarian, J. Chem. Phys. **85**, 5660 (1986).
[7] M.E. Fajardo and V.A. Apkarian, Chem. Phys. Lett. **134**, 1 (1987).
[8] R. Shriever, M. Chergui, H. Kunz, V. Stepanenko, and N. Schwentner, J. Chem. Phys. **91**, 4128 (1989).
[9] R. Shriever, M. Chergui, O. Unal, N. Schwentner, and V. Stepanenko, J. Chem. Phys. **93**, 3245 (1990).
[10] J. McCaffrey, H. Kunz, and N. Schwentner, J. Chem. Phys. **96**, 2825 (1992).
[11] H. Kunz, J. McCaffrey, R. Shreiver, and N. Schwentner, J. Chem. Phys. **94**, 1039 (1991).
[12] J. McCaffrey, H. Kunz, and N. Schwentner, J. Chem. Phys. **96**, 155 (1992).
[13] K.H. Godderz, N. Schwentner, and M. Chergui, Chem. Phys. **209**, 91 (1996).
[14] K.H. Godderz, N. Schwentner, and M. Chergui, J. Chem. Phys. **105**, 451 (1996).
[15] H. Kunttu and V.A. Apkarian, Chem. Phys. Lett. **171**, 423 (1990).
[16] A.I. Katz and V.A. Apkarian, J. Phys. Chem. **94**, 6671 (1990).
[17] E.T. Ryan and E. Weitz, J. Chem. Phys. **99**, 1004 (1993).
[18] E.T. Ryan and E. Weitz, J. Chem. Phys. **99**, 8628 (1993).
[19] D. Labrake, E.T. Ryan, and E. Weitz, J. Chem. Phys. **102**, 4112 (1995).
[20] R. Zadoyan, Z. Li, P. Ashjian, C.C. Matrtens, and V.A. Apkarian, Chem. Phys. Lett. **218**, 504 (1993).
[21] R. Zadoyan, Z. Li, C.C. Matrtens, and V.A. Apkarian, J. Chem. Phys. **101**, 6648 (1994).
[22] Z. Li, R. Zadoyan, V.A. Apkarian, and C.C. Matrtens, J. Phys. Chem. **99**, 7453 (1995).
[23] R. Fraenkel and Y. Haas, Chem. Phys. Lett. **214**, 234 (1993).
[24] R. Alimi, R.B. Gerber, and A. Brokman, *Stochasticity and Intramolecular Redistribution of Energy* (Reidel, Dordrecht, 1987), p. 233.
[25] R. Alimi, R.B. Gerber, and V.A. Apkarian, J. Chem. Phys. **89**, 174 (1988).
[26] R.B. Gerber, R. Alimi, and V.A. Apkarian, Chem. Phys. Lett. **158**, 257 (1989).

[27] R. Alimi, A. Brokman, and R.B. Gerber, J. Chem. Phys. **91**, 1611 (1989).
[28] R. Alimi, R.B. Gerber, and V.A. Apkarian, J. Chem. Phys. **92**, 3551 (1990).
[29] R. Alimi, V.A. Apkarian, and R.B. Gerber, J. Chem. Phys. **98**, 331 (1993).
[30] R. Alimi, R.B. Gerber, and V.A. Apkarian, Phys. Rev. Lett. **66**, 1295 (1991).
[31] R. Alimi, R.B. Gerber, J.G. McCaffrey, H. Kunz, and N. Schwentner, Phys. Rev. Lett. **69**, 856 (1992).
[32] R.B. Gerber and A.I. Krylov, in *Reaction Dynamics in Clusters and Condensed Phases*, edited by J. Jortner (Annual Reviews Inc., Palo Alto, CA, 1994), pp. 509–520.
[33] A.I. Krylov and R.B. Gerber, J. Chem. Phys. **100**, 4242 (1994).
[34] R.B. Gerber, A.B. McCoy, and A. Garcia-Vela, Annu. Rev. Phys. Chem. **45**, 275 (1994).
[35] H. Schroder and H. Gabriel, J. Chem. Phys. **104**, 587 (1996).
[36] A. Brokman and C.C. Martens, J. Chem. Phys. **102**, 1905 (1995).
[37] I.H. Gersonde and H. Gabriel, J. Chem. Phys. **98**, 2094 (1993).
[38] V.S. Batista and D.F. Coker, J. Chem. Phys. **105**, 4033 (1996).
[39] F.O. Ellison, J. Am. Chem. Soc. **85**, 3540 (1963).
[40] A.I. Krylov and R.B. Gerber, Chem. Phys. Lett. **2312**, 395 (1994).
[41] A.I. Krylov, R.B. Gerber, and V.A. Apkarian, J. Phys. Chem. **189**, 261 (1994).
[42] A.I. Krylov, R.B. Gerber, and R.D. Coalson, J. Chem. Phys. **105**, 4626 (1996).
[43] A.I. Krylov, R.B. Gerber, M.A. Gaveau, J.M. Mestdagh, B. Schilling, and J.P. Visticot, J. Chem. Phys. **104**, 3651 (1996).
[44] A.A. Buchachenko and N.F. Stepanov, J. Chem. Phys. **104**, 9913 (1996).
[45] M. Bettendorff, S.D. Peyerimhoff, and R.J. Buenker, Chem. Phys. **66**, 261 (1982).
[46] R.A. Aziz and M.J. Slaman, Mol. Phys. **58**, 679 (1986).
[47] R.W. Bickes, B. Lantszch, J.P. Toennies, and K. Walaschenski, Discuss. Faraday Soc. **55**, 167 (1973).
[48] V. Aquilanti, D. Cappelletti, V. Lorent, E. Luzzatti, and F. Pirani, J. Phys. Chem. **97**, 2063 (1993).
[49] J.C. Tully, J. Chem. Phys. **93**, 1061 (1990).
[50] P. Jungwirth and R.B. Gerber, J. Chem. Phys. **104**, 3651 (1996).
[51] A.I. Krylov and L.Ya. Baranov (unpublished).
[52] C.A. Mead, Rev. Mod. Phys. **64**, 51 (1992).
[53] M.P. Allen and D.J. Tildesley, *Computer Simulations of Liquids* (Clarendon, Oxford, 1987).
[54] B. Schmidt and P. Jungwirth, Chem. Phys. Lett. **259**, 62 (1996).